AIP Advances

Tuning high-Q superconducting resonators by magnetic field reorientation

Cite as: AIP Advances **9**, 125225 (2019); https://doi.org/10.1063/1.5129032
Submitted: 30 October 2019 . Accepted: 10 December 2019 . Published Online: 20 December 2019

Christoph W. Zollitsch, James O'Sullivan, Oscar Kennedy, Gavin Dold, and John J. L. Morton

Tuning high-Q superconducting resonators by magnetic field reorientation

Cite as: AIP Advances 9, 125225 (2019); doi: 10.1063/1.5129032
Submitted: 30 October 2019 • Accepted: 10 December 2019 •
Published Online: 20 December 2019

View Online Export Citation CrossMark

Christoph W. Zollitsch,[1,a)] James O'Sullivan,[1] Oscar Kennedy,[1] Gavin Dold,[1] and John J. L. Morton[1,2]

AFFILIATIONS

[1] London Centre for Nanotechnology, University College London, 17-19 Gordon Street, London WCH1 0AH, United Kingdom
[2] Department of Electronic & Electrical Engineering, UCL, London WC1E 7JE, United Kingdom

[a)] Electronic mail: c.zollitsch@ucl.ac.uk

ABSTRACT

Superconducting resonators interfaced with paramagnetic spin ensembles are used to increase the sensitivity of electron spin resonance experiments and are key elements of microwave quantum memories. Certain spin systems that are promising for such quantum memories possess "sweet spots" at particular combinations of magnetic fields and frequencies, where spin coherence times or linewidths become particularly favorable. In order to be able to couple high-Q superconducting resonators to such specific spin transitions, it is necessary to be able to tune the resonator frequency under a constant magnetic field amplitude. Here, we demonstrate a high-quality, magnetic field resilient superconducting resonator, using a 3D vector magnet to continuously tune its resonance frequency by adjusting the orientation of the magnetic field. The resonator maintains a quality factor of $>10^5$ up to magnetic fields of 2.6 T, applied predominantly in the plane of the superconductor. We achieve a continuous tuning of up to 30 MHz by rotating the magnetic field vector, introducing a component of 5 mT perpendicular to the superconductor.

Superconducting coplanar microwave resonators allow for a variety of compact designs, in conjunction with high-quality factors, and find applications in the sensitive readout of individual quantum systems and small ensembles[1–7] and the coupling of distinct physical systems.[2,8,9] Superconducting resonators inductively coupled to atomic impurity spins form the basis of proposals for spin-based quantum memories[10–14] and have led to substantial advances in the detection limit of electron spin resonance.[5–7]

The study of spins coupled to superconducting microwave resonators typically requires static magnetic fields in the range of several 100 mT to tune the spin Zeeman energy to be resonant with the resonator. Superconducting resonators often exhibit limits in the quality factor ($<10^5$) under the influence of such static magnetic fields,[15–17] and while previous studies have shown enhanced magnetic field resilience of a high-quality factor ($>10^5$),[18,19] these resonator designs were not optimized for high sensitivity spin sensing. Furthermore, of particular interest in the context of long-lived spin-based quantum memories are specific spin transitions that show an increased resilience to dominant sources of noise (e.g., magnetic or electric field noise).[20–22] Prominent examples of systems with such magnetic field noise resilient transitions include bismuth donors in silicon, where the donor electron spin coherence time reaches seconds,[20] as well as rare-earth dopants (e.g., Nd, Er, or Yb) in Y_2SiO_5[23] reaching electron spin coherence times of 1 ms.[22] In the latter case, the additional presence of robust optical transitions leads to potential applications for microwave-to-optical quantum transducers. Common to all these applications is an optimum working point, which is dictated by the spin species and sets both the magnetic field magnitude and the required resonator frequency at this given magnetic field. Matching the resonator frequency to the relevant spin transition is challenging due to fabrication uncertainties relating to film deposition and device patterning, which affect frequency reproducibility; this, indeed, is becoming a widespread challenge in the field of kinetic inductance detectors[24] and quantum circuits.[25] This challenge is further compounded by the additional frequency down-shift of the resonator due to an applied in-plane magnetic field, which needs to be accounted for before fabrication. *In situ* frequency tunable resonators offer a practical route to adjust the resonator frequency, which increases the tolerance of fabrication uncertainties, and additionally offer the ability to study a spin system across a (small) frequency range. Several methods have been demonstrated for frequency-tuning superconducting resonators, including (i) current-biasing through the signal line,[26,27] (ii) embedding SQUIDs into the resonator as magnetic-field tunable inductors,[28–30] and (iii) simply applying global magnetic fields to tune the resonator frequency.[18,31,32] None of these approaches is ideally suited to the task of achieving strong coupling to noise-resilient spin transitions: they display a magnetic field resilience that is either limited[30,32] or not investigated,[28,29] possess relatively low quality factors,[26] or rely on changing the overall magnetic field strength[18,27,31,32] (despite this value being determined by the chosen spin transition).

In this article, we present a superconducting thin-film lumped element resonator (LER) tailored for high resilience to static in-plane magnetic fields (up to 2.6 T), and show how its frequency may be tuned by introducing an additional magnetic field component, perpendicular to the superconducting thin-film. In this way, we demonstrate a frequency tunability of up to 30 MHz (arising for a perpendicular magnetic field component of 5 mT) while maintaining high-quality factors ($Q_L > 10^5$).

The resonator frequency $\omega_{res} = 1/\sqrt{LC}$, where L and C are, respectively, the inductance and capacitance of the resonator.[33] The inductance can be further divided as $L = L_G + L_{kin}$, where L_G is the geometric inductance, and L_{kin} is the kinetic inductance,[34] arising from the finite inertia of the charge carriers,[35] whose resulting effect is similar to an electromotive force on a charge in an inductor. To tune the resonator frequency, we exploit the dependence of L_{kin} on the Cooper pair density n_s, which takes the form $L_{kin} \propto 1/n_s$.[36,37] Applying a static magnetic field reduces n_s, thus tuning the resonator to lower frequencies, and as long as the applied field does not exceed the first critical field, hysteretic effects in frequency tuning can be avoided.[38]

Figure 1(a) shows a schematic of the lumped element resonator, which was designed for high field resilience by minimizing the area of the superconducting thin film. The AC electric and magnetic fields are spatially separated (see the supplementary material for finite element simulations). This allows us to concentrate on the magnetic fields around the narrow inductor wire (to strongly couple to a small number of spins) but also introduces significant radiative losses. To suppress the radiative losses, the resonator is placed inside a 3D copper cavity ($Q_{3Dcav} \approx 800$) and is excited/read-out by capacitively coupling to two antennae protruding inside the 3D cavity volume.[5] Measured in this way, resonators can demonstrate loaded quality factors exceeding 10^5.

The resonator, as shown in Fig. 1(a), has an overall dimension of 600 μm × 600 μm. The capacitor fingers are 10 μm wide, separated by 50 μm, and the total length of the outer and inner fingers is 1.6 mm and 1.35 mm, respectively. The inductor wire is 440 μm long and 2 μm wide [highlighted in yellow in Fig. 1(a)]. The resonator is fabricated by electron beam lithography and reactive ion etching into a ≈50 nm thick NbN film, sputtered on a 250 μm thick high-resistivity ($\rho > 5000\ \Omega$ cm) n-type Si substrate. The 3D cavity loaded with the LER is mounted inside a dilution refrigerator and cooled to a base temperature of 20 mK. Static magnetic fields of arbitrary orientation were applied using an American Magnetics Inc 3-axis vector magnet (see the supplementary material for further details on the used measurement setups).

Figure 1(b) shows the microwave transmission $|S_{21}|^2$ as a function of frequency at a temperature of 20 mK, with an input power at the resonator of −115 dBm and no externally applied magnetic field. The resonator response is asymmetric due to the strong impedance mismatch induced by the coupling antennae of the 3D cavity.[39,40] This can be fit by a Fano resonance[41] to extract the resonator parameters: the frequency $\omega_{res}/2\pi = 6375$ MHz and loaded quality factor $Q_L = 2.97 \times 10^5$. Figure 1(c) compares Q_L as a function of the estimated average photon number $\langle n \rangle$ in the lumped element resonator at zero applied field vs that at an applied in-plane magnetic field of 1 T. The uncertainty in $\langle n \rangle$ is about one order of magnitude and originates from our estimation of the total attenuation of the setup (supplementary material). The zero field loaded quality factor exhibits a kink at $\langle n \rangle \approx 8400$ (−120 dBm) and then continues to increase with increasing microwave power. We attribute this to the onset of nonlinearity, which is accompanied by a downward shift in frequency (see the supplementary material). The power dependent data are

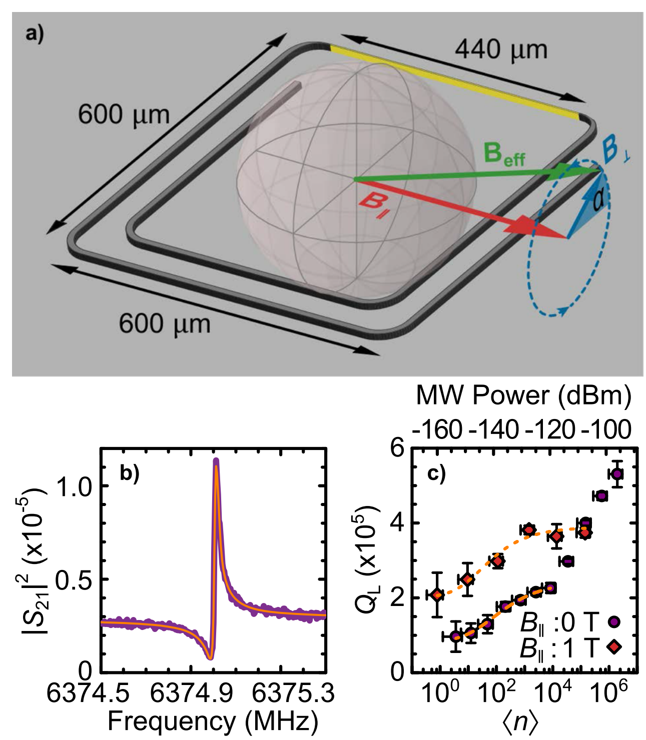

FIG. 1. (a) Schematic of the lumped element NbN thin-film resonator and the applied magnetic field B_{eff} with two components: $B_\parallel$ lies precisely in the plane of the superconducting film and nominally along the inductor wire (highlighted in yellow), while $B_\perp$ is defined perpendicular to $B_\parallel$ with an angle α to the plane of the superconducting film; to tune the resonator frequency, α is varied, while maintaining a constant magnetic field amplitude, (b) microwave transmission $|S_{21}|^2$ as a function of frequency for an input power at the LER of −115 dBm at a temperature of 20 mK, including a fit (solid orange line), and (c) the loaded quality factor Q_L as a function of the estimated average photon number in the LER at zero magnetic field (purple symbols) and a 1 T in-plane magnetic field (red diamonds). The top axis gives the corresponding microwave power at the resonator. The estimate is a coarse guide, with an uncertainty of one order of magnitude (supplementary material).

fit to a two level system (TLS) model, where the quality factor is limited by fluctuating TLSs in the substrate and at the surface[42–44] (see the supplementary material for details). The fit is performed for average photon numbers where the resonator is not in the nonlinear regime and is shown by dashed lines in Fig. 1(c). This model fits our data well, supporting the interpretation of power dependent losses. Importantly, the loaded quality factor of the resonator remains higher at 1 T than at zero field for all powers where the resonator is in the linear regime. The field dependence of the low-power TLS-limited quality factor suggests that at high field, either the TLS states become unpopulated or become detuned from the resonator. However, to fully quantify this observation, a more thorough magnetic field dependent study is required, which is beyond the scope of this article but may be relevant to the impact of TLSs on qubit coherence times.[45] From the measured resonance frequency and an estimate of the LER's capacitance, using conformal mapping techniques,[46] we determine the resonator's impedance to be $Z = 320\ \Omega \pm 20\ \Omega$.

Figure 1(a) illustrates the coordinate system we define, in which we create a total magnetic field vector B_{eff} by applying a constant in-plane field $B_\parallel$, together with a smaller perpendicular component $B_\perp$ whose angle α is varied. $B_\parallel$ is primarily responsible for setting the overall magnetic field amplitude and direction, which tunes the spin transition frequencies to be resonant with the resonator, and oriented along the inductor so that spins directly beneath the wire satisfy the electron spin resonance condition, whereby the static magnetic field is perpendicular to the oscillating microwave magnetic field. The orientation for $B_\parallel$ is roughly set along a principal axis of the vector magnet when loading the sample and then carefully aligned to be in the plane of the superconductor through an iterative process at base temperature. We apply a small field (2 mT) along the nominal $B_\parallel$ axis and then tilt the applied field out of the plane of the superconducting film. At these small fields, we can apply the field perpendicular to the resonator without degrading the resonator, and thus large tilt angles may be used. By identifying the orientation where the resonator frequency is maximized, we identify an axis which is in the plane of the superconducting thin film. We then ramp the redefined $B_\parallel$ to a larger field, and repeat this process. As the magnitude $B_\parallel$ increases, the tilt angle decreases, ensuring that large fields are not applied perpendicular to the resonator plane. During this process, we keep the perpendicular field component always smaller than 4 mT. We choose logarithmically increasing $B_\parallel$ setpoints at which we perform the tilting process and complete the alignment with 10 iterations. The duration of the procedure also depends on the magnetic field ramp-rate, which was 50 mT/min and was completed within ∼1.5 h. We followed this alignment process up to $B_\parallel = 1$ T, achieving an accuracy of the in-plane vector of 0.2%. Although this sets tight bounds on the alignment of $B_\parallel$ within the plane of the superconductor, the orientation along the inductor wire was not optimized beyond that upon sample loading. This does not affect the measurements presented here, and alignment could be performed by, e.g., maximizing an ESR echo amplitude for spins beneath the wire.

Figure 2 shows the measured resonator frequency and the loaded quality factor Q_{L} as a function of the in-plane magnetic field $B_\parallel$, while $B_\perp$ is kept at 0 T. As the static magnetic field increases from zero to $B_\parallel = 2.7$ T, the resonance frequency decreases by 245 MHz and largely follows a parabolic dispersion (solid curve), as expected from the kinetic inductance resulting from the change in the Cooper pair density n_s.[31,32,36] The parabolic dispersion only holds good for superconductors where vortex losses are not dominant, and divergence from this behavior indicates that the superconductor is predominately in its type-II state where flux vortices are the main source of loss.[47] For $B_\parallel > 2.1$ T, the resonator frequencies deviate from the parabolic function, and for $B_\parallel > 2.6$ T, a kink is observed, which we interpret as vortex losses become a dominant loss mechanism at such fields.

As $B_\parallel$ is increased from zero, Q_{L} of the resonator drops from about 3×10^5 to a minimum of about 4×10^4 at a magnetic field of 234 mT. We attribute this to the presence of paramagnetic dangling bond defects at the Si/SiO_2 (natural oxide) interface, with g-factors ≈2, inductively coupling to the resonator. Dangling bond defects[48–50] are known to have densities of $\approx 10^{12}/\mathrm{cm}^2$ and are located in close vicinity to the NbN inductor where the strongest oscillating magnetic fields are present; hence, they will strongly interact with the resonator, causing a drop in the quality factor due to their dissipation. This is consistent with recent observations on dangling bond defects with g ≈ 2 reducing the quality factor of resonators in both silicon[18] and sapphire[19,51] substrates at relevant magnetic fields. Increasing $B_\parallel$ further leads to an increase in Q_{L}, reaching a maximum of 8.6×10^5 at 1 T. This suggests that the dangling bond defects limit resonator losses even at zero magnetic field. Note that the microwave power dependence at 1 T, as shown in Fig. 1(c), is performed in a different setup where a higher field noise limits the maximal achievable Q_{L}, resulting in a lower Q_{L} than that shown in Fig. 2(b) (supplementary material). For $B_\parallel > 1$ T, the quality factor starts to decrease due to finite misalignments in the static field as the alignment procedure

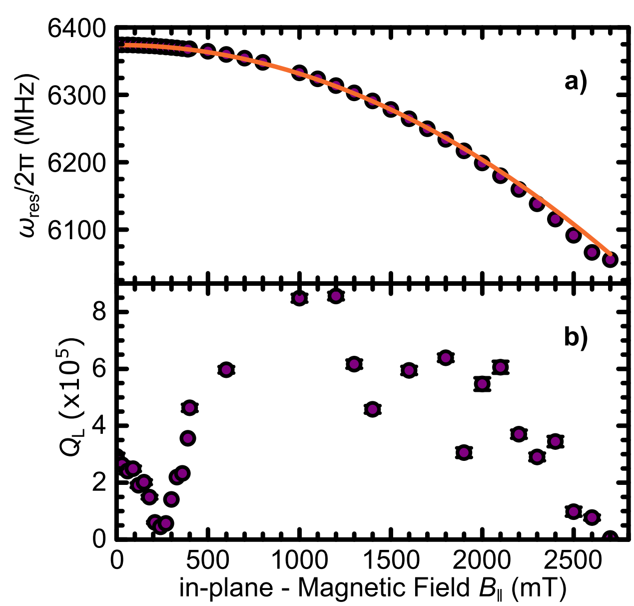

FIG. 2. (a) Extracted resonance frequency and (b) the loaded quality factor as a function of the in-plane magnetic field $B_\parallel$ at a temperature of 20 mK and an input power at the resonator of −112 dBm. The field range from 0 to 400 mT is measured with a higher resolution.

was performed only up to $B_{\parallel} = 1$ T. At fields larger than 2.5 T, Q_L falls below 10^5.

Finally, we investigate the tunability of the resonator frequency by introducing an additional field, $B_{\perp}$, and rotating it by the angle α, as shown in Fig. 1(a). $B_{\perp}$ is kept smaller than the out-of-plane critical field (estimated to be $B_{\perp,c1} \approx 6.2$ mT) to ensure nonhysteretic frequency tuning. Figure 3(a) shows the measured resonator frequency as a function of α for $B_{\perp} = 4$–6 mT at zero applied $B_{\parallel}$, as well as for $B_{\perp} = 4$ mT, with a larger in-plane $B_{\parallel} = 1$ T. After each full magnetic field rotation, the resonator is thermally cycled to 18 K to remove any trapped flux and establish a common reference. This is necessary as, although the frequency tuning is nonhysteretic, the resonator loaded quality factor does show hysteresis and does not fully recover to the 0° value when rotated by 360°, particularly for a 6 mT out-of-plane field, as shown in Fig. 3(b). The resonator frequency shows a $1 + \cos(2\alpha)$ dependence [solid lines in Fig. 3(a)], with a frequency minima for the maximal out-of-plane field. The behavior is symmetric for $B_{\perp} = 4$ mT, while some asymmetry becomes apparent for larger values for $B_{\perp}$ which we attribute to induced flux vortices. We define the variability of the resonance frequency tuning as $\frac{\omega_{\mathrm{res}}(\alpha)}{\omega_{\mathrm{res}}(\alpha+\pi)}$, which is below 0.005%, 0.015%, and 0.045% for $B_{\perp} = 4$ mT, 5 mT, and 6 mT, respectively. The maximum tuning range is 20.13(1) MHz, 30.63(3) MHz, and 41.4(1) MHz for a $B_{\perp}$ of 4 mT, 5 mT, and 6 mT, respectively. At an in-plane field of 1 T, the tuning behavior is nearly identical to the zero field case. Here, for $B_{\perp} = 4$ mT, the variability is below 0.005%, and the maximum tuning range is 19.77 ± 0.1 MHz, a reduction in the tuning range by less than 2% compared with the range at zero field.

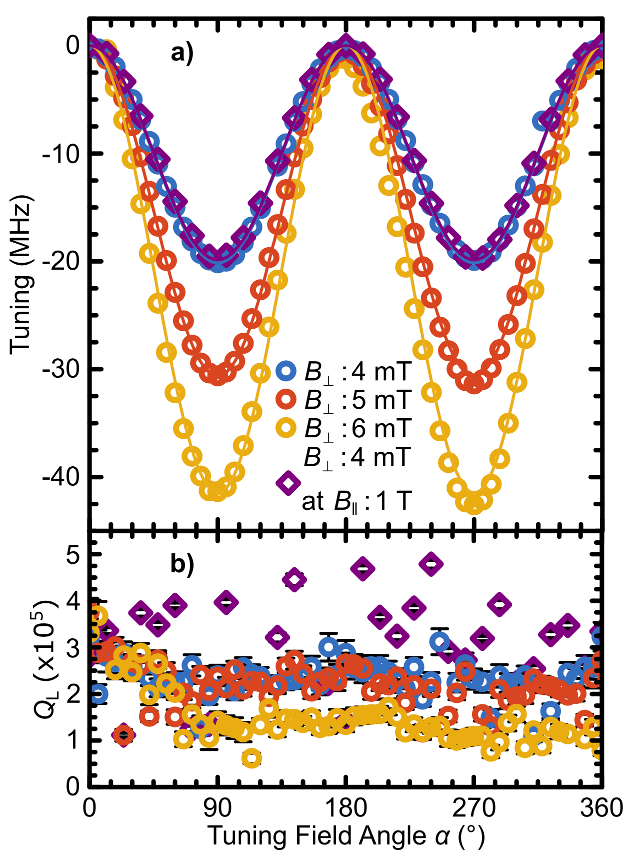

FIG. 3. (a) Extracted resonance frequency and (b) the loaded quality factor as a function of the out-of-plane magnetic field angle α at a temperature of 20 mK and an input power at the resonator of −120 dBm; the four datasets are rotations with a field magnitude of $B_{\perp}$ of 4 mT (blue circle), 5 mT (red circle), 6 mT (yellow circle), and $B_{\perp}$ of 4 mT at $B_{\parallel} = 1$ T (dark blue diamond); the solid lines in (a) show a calculated $1 + \cos(2\alpha)$ dependence of the tuning.

The loaded quality factor is shown as a function of the magnetic field angle α in Fig. 3(b) and has a value of 3.2×10^5 for the three different $B_{\perp}$ amplitudes for $\alpha = 0$, with no additional in-plane field. Rotating $B_{\perp}$ out-of-plane of the superconducting film decreases the quality factor: for 4 mT and 5 mT rotations, Q_L drops to an average value of 2.2×10^5 when α reaches 90° and remains constant for the rest of the rotation. The drop for the $B_{\perp} = 6$ mT rotation is more significant, falling to a value of 1.3×10^5 and then remaining constant. The initial drop in Q_L indicates the generation of flux vortices even at small perpendicular magnetic fields; however, for these values of $B_{\perp}$, the losses are tolerable as $Q_L > 10^5$ can be maintained, and no hysteretic behavior in resonance frequency is observed for $B_{\perp} = 4$ mT and only a small hysteretic effect, for the higher perpendicular fields. At $B_{\parallel} = 1$ T and $B_{\perp} = 4$ mT, Q_L maintains an average value of about 4×10^5. At these static in-plane magnetic fields, noise from the magnet is believed to limit the stability of the LER's resonance frequency, leading to a scatter in the measured Q_L.

Although the primary motivation of the methods presented here is the relatively slow tuning of the resonator frequency to match a desired spin transition, it is also worth reflecting on potential applications in fast-tuning of the resonator frequency within a quantum memory pulse sequence.[52] Tuning the resonator frequency by one resonator linewidth (≈28 kHz) would require $B_{\perp} \approx 140\ \mu$T, and given the maximum magnetic field ramp-rate (200 mT/min) of the magnet systems used, this could be achieved within 42 ms. Low inductance magnetic coils such as modulation coils used in conventional ESR[53] can apply magnetic fields of ∼1 mT at a frequency of 100 kHz, i.e., a 10 μs field tuning. This is considerably faster than the coherence time for spins at these magnetic fields, i.e., frequency optimal working points, and could therefore be used to tune resonators within pulse sequences for quantum memory experiments.

In summary, we presented a design for a high-quality factor, coplanar superconducting lumped element microwave resonator made of NbN, which can be operated at high static magnetic fields (up to 2.6 T in-plane of the superconductor) while maintaining a high-quality factor (>10^5). We observe a significant drop in the quality factor arising from coupling to $g \approx 2$ spins, most likely due to dangling bond defects at the Si/SiO_2 interface. We demonstrated the tuning of the resonator frequency by applying a small magnetic field perpendicular to the superconducting film, and we see near nonhysteretic frequency tuning of up to 30.63(3) MHz, while maintaining the high-quality factor. The tuning range can be further increased with higher perpendicular fields; however, the resonance frequency tuning becomes hysteretic, and the quality factor drops. A similar tuning can be performed using significant in-plane fields (e.g., 1 T). This type of resonator is therefore well suited to study the spin-resonator coupling at specific combinations of magnetic field magnitudes and resonance frequencies, e.g., magnetic field noise resilient transitions, and has a high potential for devices such as quantum memories.

See the supplementary material for a detailed description of the modeling of the resonator power dependence, the resonator fabrication finite element simulations, the experimental setups, the reproducibility of the resonator parameters between cooldowns, and a characterization of an additional device.

This research has received funding from the European Union's Horizon 2020 research and innovation program under Grant Agreement No. 688539 (MOS-QUITO), as well as from the UK Engineering and Physical Sciences Research Council, Grant No. EP/P510270/1.

REFERENCES

[1] A. Wallraff, D. I. Schuster, A. Blais, L. Frunzio, R.-S. Huang, J. Majer, S. Kumar, S. M. Girvin, and R. J. Schoelkopf, Nature **431**, 162 (2004).
[2] J. Clarke and F. K. Wilhelm, Nature **453**, 1031 (2008).
[3] A. Fragner, M. Göppl, J. M. Fink, M. Baur, R. Bianchetti, P. J. Leek, A. Blais, and A. Wallraff, Science **322**, 1357 (2008).
[4] S. E. de Graaf, A. V. Danilov, A. Adamyan, and S. E. Kubatkin, Rev. Sci. Instrum. **84**, 023706 (2013).
[5] A. Bienfait, J. J. Pla, Y. Kubo, M. Stern, X. Zhou, C. C. Lo, C. D. Weis, T. Schenkel, M. L. W. Thewalt, D. Vion, D. Esteve, B. Julsgaard, K. Moelmer, J. J. L. Morton, and P. Bertet, Nat. Nanotechnol. **11**, 253 (2016).
[6] A. Bienfait, P. Campagne-Ibarcq, A. H. Kiilerich, X. Zhou, S. Probst, J. J. Pla, T. Schenkel, D. Vion, D. Esteve, J. J. L. Morton, K. Moelmer, and P. Bertet, Phys. Rev. X **7**, 041011 (2017).
[7] S. Probst, A. Bienfait, P. Campagne-Ibarcq, J. J. Pla, B. Albanese, J. F. Da Silva Barbosa, T. Schenkel, D. Vion, D. Esteve, K. Moelmer, J. J. L. Morton, R. Heeres, and P. Bertet, Appl. Phys. Lett. **111**, 202604 (2017).
[8] X. Mi, J. V. Cady, D. M. Zajac, P. W. Deelman, and J. R. Petta, Science **355**, 156 (2017).
[9] N. Samkharadze, G. Zheng, N. Kalhor, D. Brousse, A. Sammak, U. C. Mendes, A. Blais, G. Scappucci, and L. M. K. Vandersypen, Science **359**, 1123 (2018).
[10] J. H. Wesenberg, A. Ardavan, G. A. D. Briggs, J. J. L. Morton, R. J. Schoelkopf, D. I. Schuster, and K. Mølmer, Phys. Rev. Lett. **103**, 070502 (2009).
[11] H. Wu, R. E. George, J. H. Wesenberg, K. Mølmer, D. I. Schuster, R. J. Schoelkopf, K. M. Itoh, A. Ardavan, J. J. L. Morton, and G. A. D. Briggs, Phys. Rev. Lett. **105**, 140503 (2010).
[12] C. Grezes, B. Julsgaard, Y. Kubo, M. Stern, T. Umeda, J. Isoya, H. Sumiya, H. Abe, S. Onoda, T. Ohshima, V. Jacques, J. Esteve, D. Vion, D. Esteve, K. Mølmer, and P. Bertet, Phys. Rev. X **4**, 021049 (2014).
[13] C. Grezes, B. Julsgaard, Y. Kubo, W. L. Ma, M. Stern, A. Bienfait, K. Nakamura, J. Isoya, S. Onoda, T. Ohshima, V. Jacques, D. Vion, D. Esteve, R. B. Liu, K. Mølmer, and P. Bertet, Phys. Rev. A **92**, 020301 (2015).
[14] J. J. Morton and P. Bertet, J. Magn. Reson. **287**, 128 (2018).
[15] D. Bothner, T. Gaber, M. Kemmler, D. Koelle, and R. Kleiner, Appl. Phys. Lett. **98**, 102504 (2011).
[16] S. E. de Graaf, A. V. Danilov, A. Adamyan, T. Bauch, and S. E. Kubatkin, J. Appl. Phys. **112**, 123905 (2012).
[17] S. Kwon, A. Fadavi Roudsari, O. W. B. Benningshof, Y.-C. Tang, H. R. Mohebbi, I. A. J. Taminiau, D. Langenberg, S. Lee, G. Nichols, D. G. Cory, and G.-X. Miao, J. Appl. Phys. **124**, 033903 (2018).
[18] N. Samkharadze, A. Bruno, P. Scarlino, G. Zheng, D. P. DiVincenzo, L. DiCarlo, and L. M. K. Vandersypen, Phys. Rev. Appl. **5**, 044004 (2016).
[19] J. Kroll, F. Borsoi, K. van der Enden, W. Uilhoorn, D. de Jong, M. Quintero-Pérez, D. van Woerkom, A. Bruno, S. Plissard, D. Car, E. Bakkers, M. Cassidy, and L. Kouwenhoven, Phys. Rev. Appl. **11**, 064053 (2019).
[20] G. Wolfowicz, A. M. Tyryshkin, R. E. George, H. Riemann, N. V. Abrosimov, P. Becker, H.-J. Pohl, M. L. W. Thewalt, S. A. Lyon, and J. J. L. Morton, Nat. Nanotechnol. **8**, 561 (2013).
[21] K. J. Morse, R. J. S. Abraham, A. DeAbreu, C. Bowness, T. S. Richards, H. Riemann, N. V. Abrosimov, P. Becker, H.-J. Pohl, M. L. W. Thewalt, and S. Simmons, Sci. Adv. **3**, e1700930 (2017).
[22] A. Ortu, A. Tiranov, S. Welinski, F. Froewis, N. Gisin, A. Ferrier, P. Goldner, and M. Afzelius, Nat. Mater. **17**, 671 (2018).
[23] G. Dold, C. W. Zollitsch, J. O'Sullivan, S. Welinski, A. Ferrier, P. Goldner, S. de Graaf, T. Lindström, and J. J. Morton, Phys. Rev. Appl. **11**, 054082 (2019).
[24] S. McHugh, B. A. Mazin, B. Serfass, S. Meeker, K. O'Brien, R. Duan, R. Raffanti, and D. Werthimer, Rev. Sci. Instrum. **83**, 044702 (2012).
[25] Y. Chen, D. Sank, P. O'Malley, T. White, R. Barends, B. Chiaro, J. Kelly, E. Lucero, M. Mariantoni, A. Megrant, C. Neill, A. Vainsencher, J. Wenner, Y. Yin, A. N. Cleland, and J. M. Martinis, Appl. Phys. Lett. **101**, 182601 (2012).
[26] A. T. Asfaw, A. J. Sigillito, A. M. Tyryshkin, T. Schenkel, and S. A. Lyon, Appl. Phys. Lett. **111**, 032601 (2017).
[27] A. A. Adamyan, S. E. Kubatkin, and A. V. Danilov, Appl. Phys. Lett. **108**, 172601 (2016).
[28] A. Palacios-Laloy, F. Nguyen, F. Mallet, P. Bertet, D. Vion, and D. Esteve, J. Low Temp. Phys. **151**, 1034 (2008).
[29] M. Sandberg, C. M. Wilson, F. Persson, T. Bauch, G. Johansson, V. Shumeiko, T. Duty, and P. Delsing, Appl. Phys. Lett. **92**, 203501 (2008).
[30] O. Kennedy, J. Burnett, J. Fenton, N. Constantino, P. Warburton, J. Morton, and E. Dupont-Ferrier, Phys. Rev. Appl. **11**, 014006 (2019).
[31] J. E. Healey, T. Lindström, M. S. Colclough, C. M. Muirhead, and A. Y. Tzalenchuk, Appl. Phys. Lett. **93**, 043513 (2008).
[32] M. Xu, X. Han, W. Fu, C.-L. Zou, and H. X. Tang, Appl. Phys. Lett. **114**, 192601 (2019).
[33] D. M. Pozar, *Microwave Engineering* (John Wiley and Sons, Inc., New York, 1998).
[34] M. Goeppl, A. Fragner, M. Baur, R. Bianchetti, S. Filipp, J. M. Fink, P. J. Leek, G. Puebla, L. Steffen, and A. Wallraff, J. Appl. Phys. **104**, 113904 (2008).
[35] M. Tinkham, *Introduction to Superconductivity* (McGraw-Hill, New York, 1975).
[36] W. J. Wallace and R. H. Silsbee, Rev. Sci. Instrum. **62**, 1754 (1991).
[37] K. Watanabe, K. Yoshida, T. Aoki, and S. Kohjiro, Jpn. J. Appl. Phys., Part 1 **33**, 5708 (1994).
[38] D. Bothner, T. Gaber, M. Kemmler, D. Koelle, R. Kleiner, S. Wünsch, and M. Siegel, Phys. Rev. B **86**, 014517 (2012).
[39] K. Geerlings, S. Shankar, E. Edwards, L. Frunzio, R. J. Schoelkopf, and M. H. Devoret, Appl. Phys. Lett. **100**, 192601 (2012).
[40] M. S. Khalil, M. J. A. Stoutimore, F. C. Wellstood, and K. D. Osborn, J. Appl. Phys. **111**, 054510 (2012).
[41] U. Fano, Phys. Rev. **124**, 1866 (1961).
[42] J. Goetz, F. Deppe, M. Haeberlein, F. Wulschner, C. W. Zollitsch, S. Meier, M. Fischer, P. Eder, E. Xie, K. G. Fedorov, E. P. Menzel, A. Marx, and R. Gross, J. Appl. Phys. **119**, 015304 (2016).
[43] J. Burnett, J. Sagar, O. W. Kennedy, P. A. Warburton, and J. C. Fenton, Phys. Rev. Appl. **8**, 014039 (2017).
[44] J. Burnett, A. Bengtsson, D. Niepce, and J. Bylander, J. Phys.: Conf. Ser. **969**, 012131 (2018).
[45] J. J. Burnett, A. Bengtsson, M. Scigliuzzo, D. Niepce, M. Kudra, P. Delsing, and J. Bylander, npj Quantum Inf. **5**, 54 (2019).
[46] S. Gevorgian, L. J. P. Linner, and E. L. Kollberg, IEEE Trans. Microwave Theory Tech. **43**, 772 (1995).
[47] C. Song, T. W. Heitmann, M. P. DeFeo, K. Yu, R. McDermott, M. Neeley, J. M. Martinis, and B. L. T. Plourde, Phys. Rev. B **79**, 174512 (2009).
[48] H. Huebl, F. Hoehne, B. Grolik, A. R. Stegner, M. Stutzmann, and M. S. Brandt, Phys. Rev. Lett. **100**, 177602 (2008).
[49] D. Pierreux and A. Stesmans, Phys. Rev. B **66**, 165320 (2002).
[50] P. M. Lenahan and J. F. Conley, J. Vac. Sci. Technol., B **16**, 2134 (1998).
[51] S. E. de Graaf, A. A. Adamyan, T. Lindström, D. Erts, S. E. Kubatkin, A. Y. Tzalenchuk, and A. V. Danilov, Phys. Rev. Lett. **118**, 057703 (2017).
[52] Y. Kubo, C. Grezes, A. Dewes, T. Umeda, J. Isoya, H. Sumiya, N. Morishita, H. Abe, S. Onoda, T. Ohshima, V. Jacques, A. Dréau, J.-F. Roch, I. Diniz, A. Auffeves, D. Vion, D. Esteve, and P. Bertet, Phys. Rev. Lett. **107**, 220501 (2011).
[53] C. P. Poole, Jr., *Electron Spin Resonance: A Comprehensive Treatise on Experimental Techniques* (Dover Publications, 1997).